ARTICLE

Check for updates

Panarctic lakes exerted a small positive feedback on early Holocene warming due to deglacial release of methane

L. S. Brosius [1✉], K. M. Walter Anthony [1], C. C. Treat[2], M. C. Jones [3], M. Dyonisius[4] & G. Grosse [2]

Climate-driven permafrost thaw can release ancient carbon to the atmosphere, begetting further warming in a positive feedback loop. Polar ice core data and young radiocarbon ages of dissolved methane in thermokarst lakes have challenged the importance of this feedback, but field studies did not adequately account for older methane released from permafrost through bubbling. We synthesized panarctic isotope and emissions datasets to derive integrated ages of panarctic lake methane fluxes. Methane age in modern thermokarst lakes (3132 ± 731 years before present) reflects remobilization of ancient carbon. Thermokarst-lake methane emissions fit within the constraints imposed by polar ice core data. Younger, albeit ultimately larger sources of methane from glacial lakes, estimated here, lagged those from thermokarst lakes. Our results imply that panarctic lake methane release was a small positive feedback to climate warming, comprising up to 17% of total northern hemisphere sources during the deglacial period.

[1] Water and Environmental Research Center, University of Alaska Fairbanks, Fairbanks, AK, USA. [2] Permafrost Research Section, Alfred Wegener Institute Helmholtz Centre for Polar and Marine Research, Potsdam, Germany. [3] U.S. Geological Survey, Florence Bascom Geoscience Center, Reston, VA, USA. [4] Niels Bohr Institute, University of Copenhagen, Copenhagen, Denmark. ✉email: lsbrosius@alaska.edu

T he Arctic is warming four times faster than the entire globe[1], and predicted warming will continue this trend. A projected global temperature increase of 4 °C by 2100 (equivalent to 8 °C in the Arctic, SSP5-8.5)[2] threatens permafrost region soils, which cover 24% of the northern hemisphere (NH) land surface and store twice as much carbon as the atmosphere[3]. As permafrost warms and thaws, soil organic carbon previously sequestered from the atmosphere for thousands of years becomes available for microbial decomposition, resulting in enhanced release of carbon dioxide and methane (CH_4). The projected release of these greenhouse gases from thawing permafrost (92 ± 17 Pg C by 2100, RCP8.5)[4] poses a positive feedback that could accelerate warming and impede ongoing climate change mitigation and adaptation efforts[5].

The likelihood of permafrost carbon feedback to climate warming has recently been challenged by new radiocarbon analysis of methane from Antarctic glacial ice[6]. The last deglaciation (18 to 10 ka) was an 8000-year period over which global air temperature increased 6 °C[7,8] and atmospheric methane nearly doubled[9,10]. Within that period, two distinct events of abrupt warming at 14.7 ka (Bölling-Alleröd warming) and 11.6 ka (Preboreal warming) were associated with abrupt (decade-to-century scale) increases in atmospheric methane concentration (AMC). During these periods of abrupt AMC rise, Dyonisius et al.[6] found little change in the radiocarbon age of global atmospheric methane. They concluded that since methane release from ^{14}C-depleted carbon sources, such as old permafrost and hydrates, responded minimally to deglacial warming, these sources will be unimportant in scenarios of future warming. This conclusion was corroborated by other recent studies reporting contemporary radiocarbon ages of methane dissolved in Arctic thermokarst lakes[11,12]; however, these studies did not account for the relatively older $^{14}CH_4$ age of lake bubbles, particularly those formed in deeper thawing permafrost layers of carbon-rich Pleistocene-aged yedoma soils[13], the domain of which extended across ~2.6 million square kilometers of north Siberia, Alaska, and northwest Canada during the late Pleistocene[14].

Here we examine the contribution of permafrost carbon sources to the AMC during the last deglaciation using an independent approach that is more direct than inferring northern permafrost sources from analyses of Antarctic ice. We synthesized 154 published radiocarbon ages of diffusive and ebullitive methane emissions from present-day panarctic lakes[15] and applied these ages to modeled lake methane emissions based on an extensive new paleoenvironmental dataset of 1207 northern lake initiation ages[16]. This yielded a bottom-up reconstruction of lake methane emissions and their radiocarbon values from 18 ka to the present (Methods), which we then compared to top-down estimates based on ice core models.

Thermokarst lakes constitute the most widespread form of abrupt thaw in the panarctic[17], and the most efficient means of rapidly (over decades to centuries) mobilizing old carbon by deep permafrost thaw[18–21]. However, in addition to thermokarst lake emissions, we also calculated emissions from glacial lakes since they (1) emit ^{14}C-depleted methane[19]; (2) dominate panarctic lake area (i.e., glacial lakes comprise >75% of all lakes north of 45° by both number and area[22]); and (3) represent a cryosphere response to warming[23]. Our new dataset increases the number and type of lake initiation records previously used to reconstruct deglacial lake methane emission dynamics[24,25] by >10-fold (Fig. S1). In addition to 162 thermokarst lake initiation dates, it includes 921 glacial lake records, and 124 dates from lakes of other or unknown origin. Altogether, these lake initiation data span the entire spatial domain characterized by past permafrost and glaciations during the Last Glacial/Permafrost Maximum in the northern hemisphere[26] (Fig. 1). This domain expands well

beyond the present-day permafrost extent and represents extensive lake-rich regions that were not included in past thermokarst lake methane reconstructions for Beringia[24,25]. We hereafter refer to the lakes within this study domain as "panarctic." To our knowledge, this is the first study to specifically estimate methane contributions from glacial lakes distinctly from boreal peatlands, thermokarst lakes, and other northern (>30°N) sources. Aggregated, all northern sources comprised up to 30% of the global atmospheric methane source during the deglacial period[27,28].

Despite inescapable uncertainties associated with reconstructing past phenomena, we here present estimates of deglacial to present-day panarctic lake methane emissions based on the best available data. We have attempted to address probable uncertainties where possible, and discuss additional sources of error that we were unable to quantify due to their complexity or a lack of data (Supplementary Information Section 1). We acknowledge uncertainty with respect to the absolute magnitude and timing of estimated emission values, but maintain that our data support important conclusions regarding the function of thermokarst lakes as a positive feedback to deglacial climate warming. We furthermore highlight factors we suspect may have had a potentially significant influence on past lake emission strengths, and introduce opportunities to resolve data gaps that currently prevent better model accuracy.

Results
Patterns of lake formation. Across the entire deglacial period, climate fluctuations impacted landscape-level deglaciation, permafrost degradation, and the associated lake-forming processes[23]. Panarctic lake formation pre-dated rapid peatland expansion[29] by ~2000 years and followed an increase in NH summer insolation[30] and temperature inferred from Greenland ice $\delta^{18}O$[31] (Fig. 2). Two peaks in panarctic lake formation (13.2 ka and 10.4 ka, Fig. 2b) were separated by a brief decline synchronous with cooling during the Younger Dryas (12.9–11.6 ka). Thermokarst Lake formation, specifically, appears to have been driven by increases in temperature and changes in water balance towards the wetting of permafrost landscapes, which accelerated and amplified ground ice melt[23]. Our dataset reveals that thermokarst lake formation increased quickly and strongly following the onset of both warming periods (though more so with sustained Preboreal warming) (Fig. 2c), suggesting that permafrost responded rapidly to changing climate conditions. Glacial lake formation, dependent on regressive melt of glaciers and ice sheets with high thermal inertia, responded more gradually to climate fluctuations in both directions (Fig. 2c). Widespread glacial lake formation was likely driven by ice sheet recession that exposed large areas of the land surface to associated lake-forming processes such as inundation of glacially carved depressions, water impoundment by depositional features, melt of buried remnant glacial ice, and basin isolation by isostatic adjustment of the Earth's crust[23].

Subsequently, total panarctic lake formation decreased dramatically between 10 ka and 8 ka despite sustained early Holocene warmth (Fig. 2b). In permafrost regions, cumulative fragmentation of original, ice-rich uplands by thermokarst lake formation, modification, and drainage, likely increased overall landscape relief and drainage capacity throughout the deglacial period[23]. Development of a highly incised landscape[32] would have strongly controlled lake size and persistence over time, since forming or expanding lakes would have been increasingly likely to drain via pre-existing slopes or channels[18,33]. As lake formation decreased from 10 to 8 ka, major ice sheets also approached their minimum extents[34,35]. The deceleration of glacial lake formation during the early Holocene is therefore attributed to the evolution of landscapes from high-energy proglacial environments to more
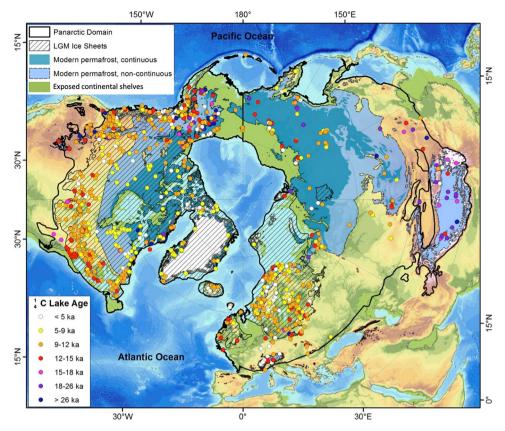
Fig. 1 Panarctic map of the cryosphere and lake basal ages. The panarctic domain (poleward of the solid black line) is defined as the combined regions affected by the Last Permafrost Maximum permafrost extent[26] (unhatched), the Last Glacial Maximum (LGM) ice sheets[70] (hatched), and exposed continental shelves during LGM[82] (green). Within this domain, the modern continuous permafrost extent (aqua) and non-continuous permafrost extent (blue)[69]. Locations of basal age records (circles) are color-coded by age.
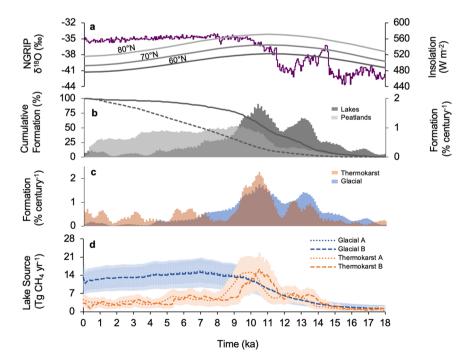

Fig. 2 Panarctic lake and peatland formation relative to climate indicators from 18 ka to present. Average summer insolation[30] (gray lines) at high northern latitudes and Greenland ice core $\delta^{18}O_{H2O}$[31] (purple) (**a**). Binned and cumulative distributions of lakes[16] (dark gray, $n = 1112$) and boreal peatland[29] ($n = 3612$, light gray) basal ages (**b**). Formation rates for glacial (blue) and thermokarst (red) lake types[23] (**c**). Methane emissions estimates with temporal uncertainty shown by dual curves A and B, (this study; scenarios explained in Methods)[81] and corresponding 1σ error (SD) envelopes for glacial (blue) and thermokarst (pink) lake types (**d**).
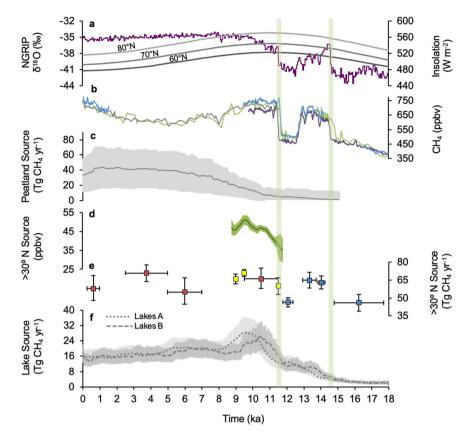
Fig. 3 Lake methane emissions in relation to polar ice core records. Northern high latitude average summer insolation[30] (gray) and Greenland ice core $\delta^{18}O_{H2O}$[31] (purple) (**a**). Atmospheric methane concentrations from GISP2 (green)[9], WAIS Divide[10] (purple), GISP (gray)[83], and NEEM[84,85] (blue) ice cores (**b**). Methane emissions from northern peatlands[29] (gray) (**c**). Northern (>30°N) source contributions to AMC inferred from the interpolar gradient[28] (green) (**d**). Discrete northern (>30°N) source AMC contributions (mean ± SD) inferred from the interpolar gradient by ref. [54] (red), ref. [27] (blue), and ref. [28] (yellow) (**e**). Total methane emissions estimated from all panarctic lakes, with temporal uncertainty shown by dual scenarios A (dotted line) and B (dashed line) with corresponding 1σ (SD) error envelopes (light gray and dark gray, respectively) in this study[81]; scenarios explained in Methods), (**f**). Vertical light-green shaded bars highlight short periods of rapid atmospheric methane increase from (**b**).

stable periglacial environments[23]. Rates of panarctic lake establishment continued to decrease steadily from 8 to 4 ka, and were much lower from 4 ka to present (Fig. 2b).

Lake methane emission estimates. Combining our lake initiation dataset with lake-type specific areal methane flux rates scaled to reflect changing temperatures[36], and constraining total allowable permafrost carbon mineralization in thermokarst lakes following a mass-balance approach[37] (Methods), we found that peak thermokarst lake emissions of 15 ± 6 Tg CH$_4$ yr^{-1} preceded peak emissions from glacial and other non-thermokarst lake types (hereafter simplified to "glacial lakes"; 15 ± 5 Tg CH$_4$ yr^{-1} at 7 ka) (Fig. 2d). Thermokarst lake emissions comprised the majority of the panarctic lake flux during portions of the deglacial period. However, glacial lakes, which dominate the panarctic lake area today, and which were not included in previous estimates of northern lake emissions since the LGM[24,25], ultimately exceeded thermokarst lake emissions by between 10 and 9 ka. Emissions from glacial lakes were more than double those from thermokarst lakes over the Holocene (Fig. 2d). Combined, the peak in panarctic lake emissions (23–28 Tg CH$_4$ yr^{-1} between 10.5 and 9 ka) preceded peak northern peatland emissions[29] by ~8000 years; however, maximum emissions from panarctic lakes appear to have lagged abrupt increases in atmospheric methane at 14.7 ka and 11.6 ka by at least 500 years (Fig. 3). While methane release resulting from a rapid expansion of lake area following the Younger Dryas (Fig. 2) accounted for up to 55% of the increase in

AMC attributed to northern sources over several millennia (12–9.5 ka)[27,28], partitioning of latitudinal sources across periods of abrupt AMC rise is still poorly resolved. Sharp increases in the AMC preceding gradual increases in both northern lake and peatland emissions, imply that other methane sources may have driven these abrupt changes.

Our estimate of present-day panarctic lake emissions (16-18 Tg CH$_4$ yr^{-1}; Fig. 3f) is similar to total northern lake methane emissions independently estimated from modern lake flux measurements applied to present-day lake areas (7–25 Tg CH$_4$ yr^{-1})[38] and estimates utilizing satellite data for parameterizing ice-free season length (13.8–17.7 Tg CH$_4$ yr^{-1})[39].

Composite age of modern lake emissions. The radiocarbon age of methane emitted from lakes is a function of emission mode and lake type. In open-water lake areas, major emission modes include ebullition and diffusion, as well as the time-delayed release of both ice-trapped bubbles and dissolved gas at ice-off (Fig. 4). Summertime diffusive fluxes and background ebullition originate largely from surface lake sediments, where predominately contemporary organic carbon substrates fuel methanogenesis when surface sediments heat up in summer. In contrast, point-source and hotspot ebullition seeps represent free-phase gas emissions channelled by bubble tubes that plumb methane formed in sequentially deeper (older) sediments[40]. In winter, surface sediments cool, slowing methanogenesis; however, the thermal lag of summer heat propagation to deeper sediments
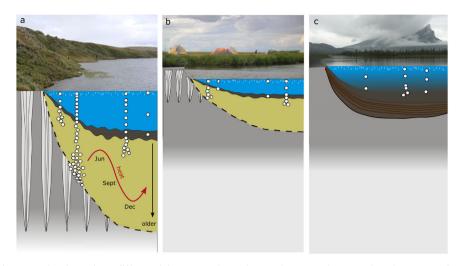
Fig. 4 Schematic of methane evasion from three different lake types. Thermokarst Lake situated in ice-rich yedoma permafrost shows a higher ratio of ebullitive (white bubbles) to diffusive (near-surface vertical dashes) fluxes, increasing age of permafrost carbon substrate with thaw bulb (tan area) depth, seasonal propagation of heat into deeper sediments stimulating microbial activity (red curve), and higher rates of methane production near the active thermokarst lake margin (**a**). Thermokarst Lake is situated in thinner, younger non-yedoma permafrost soil showing a lower ratio of ebullitive to diffusive fluxes, and shallower thaw bulb due to less ground ice content (**b**). Glacial lake surrounded by non-yedoma permafrost or unfrozen ground showing diffusive and ebullitive fluxes and laminated inorganic and Holocene-aged organic sediments (dark brown) fueling methanogenesis (**c**).

allows methanogenesis to continue through winter in talks (thaw bulbs), allowing lakes with abundant point-source and hotspot emission of ^{14}C-depleted methane to persist throughout the year[15,41,42] (Fig. 4a). In winter, bubbles escaping sediments may be temporarily impeded by seasonal ice cover. Some ^{14}C-depleted methane diffuses from bubbles resting under the ice into the water column, where its fate is methanotrophy or evasion to the atmosphere during spring ice melt[43]. The rest of the ice-trapped bubbles escape periodically during winter through ice cracks or upon degradation of the ice cover in spring[43]. These modes of emission have been summarized for ~140 panarctic lakes[38,41,44,45] and are presented according to lake type (yedoma vs. non-yedoma thermokarst lakes, glacial lakes) in Table S1.

The radiocarbon age of methane in bubbles has been shown to have a 1:1 relationship with permafrost soil carbon ages[19] and is dependent on the type of geologic substrates in which lakes form and the depth of sediments in which methane is produced. Approximately 64% of total annual emissions from lakes formed in thick (average thickness 25 m) late Pleistocene yedoma permafrost deposits occur via point source and hotspot ebullition. Relatively old ^{14}C-CH_4 ages observed in yedoma lake point-source bubbles (13,000 to 42,900 yr BP) reflect methane formed deep within the anaerobic taliks[40]. Since carbon-rich soils surrounding non-yedoma thermokarst lakes and glacial lakes are thinner (usually <3 m) and younger (Holocene-aged)[19], point-source ebullition is less common, diffusive emissions are relatively more important, and the radiocarbon ages of emitted methane in both bubbles and dissolved gases is substantially younger than in yedoma lakes.

Our synthesis of published methane radiocarbon ages and emission modes (diffusion, storage, ebullition) for panarctic lakes[15] revealed that ebullition-derived fluxes with a mean age of 9030 ± 5559 yr BP (mean ± SD) dominated emissions in thermokarst lakes formed in Pleistocene-aged yedoma permafrost soils (Table 1). Summertime diffusive fluxes, and those at ice-out, were 9 and 2% of emissions from these lakes, respectively, but the ^{14}C age of dissolved gases in surface lake water was 1713 ± 1407 yr BP in summer, and 1713 ± 3120 yr BP in spring under ice, yielding a net annual radiocarbon age of total emissions of 7828 yr BP (Table 1). Comparing seasonal ages of methane dissolved in the

surface water of interior Alaska yedoma lakes, summer ages were younger (1490 yr BP) than spring ages (2226 yr BP) because bubbles containing older methane contribute to the dissolved gas pool below ice in winter[43,46] and summertime heating of surface sediments enhances methanogenesis from younger substrates[40].

Diffusive fluxes comprise proportionately more of annual emissions from glacial (20%) and non-yedoma (30%) thermokarst lakes compared to yedoma lakes (9%). In these lakes, the [14]CH_4 ages of both bubbles and dissolved gas were younger than in yedoma lakes (Table 1), yielding net [14]CH_4 ages of 1849 yr BP and 1984 yr BP for glacial and non-yedoma thermokarst lakes, respectively. As with yedoma lakes, [14]CH_4 was younger in the surface water in summer than in spring, under the lake ice. Weighting emissions by lake area and emission modes, the net ages of total panarctic lake emissions and thermokarst lake emissions were 1978 ± 1226 yr BP and 3132 ± 731 yr BP, respectively (Table 1). These ages represent a mixture of methane formed from contemporary and old substrates, but their net age being thousands of years older than modern carbon, indicates the importance of ancient carbon mobilization and release to the atmosphere.

Radiocarbon mixing model results. To compare our bottom-up estimates with top-down constraints from atmospheric $\Delta^{14}CH_4$ measurements in ice cores, we re-ran the atmospheric CH_4 box model of Dyonisius et al.[6] in a forward model scheme (Methods) using our reconstructed thermokarst lake emissions as input. We assumed that thermokarst lakes constituted the majority of emissions from permafrost systems because they are the most efficient means for the deep thaw of ^{14}C-depleted permafrost substrates[20]. For the ^{14}C activity of the thermokarst lake emissions, we used both the composite age of all thermokarst lake emissions (3132 yr BP) and yedoma thermokarst lake emissions (7828 yr BP) reported in this study. Our use of the two end members (3132 yr BP and 7828 yr BP) accounts for the impact of any spatiotemporal fluctuation in emitted methane radiocarbon ages over time. Figure 5 shows the expected atmospheric $\Delta^{14}CH_4$ during the last deglaciation, given our bottom-up thermokarst lake emissions. Though contemporary emissions appear most compatible, our bottom-up emissions are within the uncertainty

Table 1 Lake areas, the relative contribution of emission modes to total annual methane emissions, and methane emission ^{14}C ages (mean ± SD in yrs BP) compiled from published literature[15].

	Lake Type									
	Yedoma Thermokarst		Non-yedoma Thermokarst		Glacial lakes		All Panarctic		Thermokarst lakes	
	Area (10³ km²)									
Present-day	41		117		1299		1457		158	
Pan-arctic fration	3%		8%		89%					
Thermokarst fraction	26%		74%							
	Fraction of total annual emission									
Diffusion	9%		30%		20%					
Storage	2%		8%		5%					
Ebullition	89%		61%		75%					
	[14]C_CH4 Age (yrs BP)									
	mean	±	mean	±	mean	±	mean	±	mean	±
Diffusion	1713	1407	304	742	ND	ND				
Storage	1713	3120	742	1047	ND	ND				
Ebullition	9030	5559	3178	1148	2399	2001				
All modes	7828	3899	1984	657	1849	1362	1978	1226	3132	731

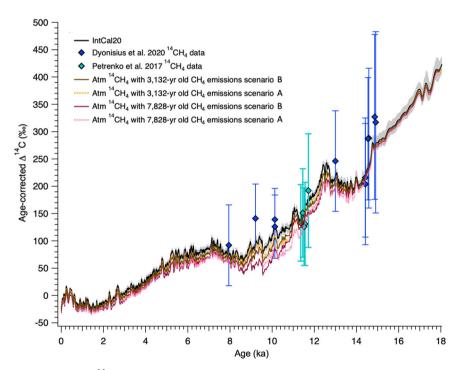A summary of emission modes by lake type are provided in Table S1.
ND no data.

Fig. 5 Comparison of expected atmospheric Δ[14]CH4 based on bottom-up thermokarst lake emission estimates A and B with published ice core Δ[14]CH4 data. Ice core data and the IntCal20 curve representing the contemporary radiocarbon age of atmospheric CO_2 are presented on their respective timescales (black line). [14]CH4 data from ice core studies are shown as blue[6]—and aqua[47]-filled diamonds. Expected atmospheric Δ[14]CH4 based on bottom-up thermokarst lake emission estimates for scenario A using [14]CH4 from lakes with a mean age of 3132 yrs (dotted yellow line) and 7828 yrs (dotted pink line). Expected atmospheric Δ[14]CH4 based on bottom-up thermokarst lake emission estimates for scenario B using [14]CH4 from lakes with a mean age of 3132 yrs (solid brown line) and 7828 yrs (solid red line). Error bars represent the 95% confidence interval.

range of ice core Δ[14]CH4 data[6,47] when the modern composite thermokarst lake emission age of 3132 years is applied, but nearer the lower limit of the uncertainty range when the older age, representing yedoma-region thermokarst lake emissions, is employed.

Discussion

Lake response to deglacial climate warming. Our study presents the first bottom-up estimate of comprehensive panarctic lake methane emissions since the Last Glacial Maximum. It includes not only thermokarst lakes, which dominated panarctic lake emissions during deglaciation, but also glacial lakes, which subsequently became more abundant and surpassed thermokarst lakes in emissions during the Holocene. Today, the entirety of glacial lakes emits more than twice as much methane as all thermokarst lakes. The northern lake methane source is also clearly distinct from the later-initiating boreal peatland source[29]; still, it does not account for the northern fraction of abrupt AMC

increases during the Last Deglaciation, and could not unless lakes consistently initiated 500–1000 years earlier than indicated by records in our dataset[16]. This suggests that processes other than the northern lake and peatland formation were responsible for the abrupt AMC rise, and supports the hypothesis that strong tropical sources (30°S–30°N), possibly in combination with smaller, yet-unidentified northern sources, drove abrupt increases in AMC that occurred during the last deglacial period[10,48,49]. Methane produced by inundation and thaw of extralimital permafrost deposits in association with sea level rise[50], thinning and northward contraction of permafrost areas in response to warming[51,52], and formation of vast proglacial lakes by ice sheet retreat[34,53] may have comprised additional northern sources. We excluded large ice-dammed, proglacial lakes from our dataset and subsequent lake area and methane emission estimates due to their high spatiotemporal complexity. This exclusion likely makes our estimates of methane emissions during phases of expanding large proglacial lakes conservative; and further study of this potential source is needed.

Variations in the panarctic lake methane flux broadly correspond with changing northern (>30°) source contributions to the AMC implied by the interpolar gradient. A ~25 Tg CH_4 yr^{-1} increase in the northern source between 12 and 9.5 ka[27,28], and an ~11 Tg CH_4 yr^{-1} decrease culminating at 6 ka[28,54], coincide with changes in panarctic lake emissions. An increase of ~14 Tg CH_4 yr^{-1}, and a subsequent decrease of ~8 Tg CH_4 yr^{-1} (Fig. 3) in lake emissions account for 55% and 73% of the changes in AMC attributed to northern (>30°) sources over these multi-millennial periods. Later methane emissions resulting from the expansion of northern peatlands likely dominated northern sources for the majority of the Holocene[29], while panarctic lake emissions continued to stabilize or decrease from 8 ka until present (Fig. 3f). The discrepancy between stable to slightly increasing lake methane emissions and decreasing northern source estimates during the Younger Dryas (Fig. 3) could have been caused by a simultaneous reduction in the strength of a yet-unconstrained northern source, persistence of lake formation under cooler climate conditions, or an inadequacy of our methods to account for the full effect of regional climate change on methane production in lakes during the Younger Dryas. Another possible explanation is the effect of dust contamination on the Greenland ice core record, which compromises the reliability of the interpolar gradient during colder climate regimes[55].

Potential variation of thermokarst lake $\Delta^{14}CH_4$. Lacking actual thermokarst lake $\Delta^{14}CH_4$ data for the last deglacial and Holocene, we used two end members (3132 yr BP, representing the age of total modern thermokarst lake emissions, and 7828 yr BP, representing the age of modern yedoma-region thermokarst lake emissions) to account for variation in emitted methane radiocarbon ages over time. Such variation could have arisen from (1) increased mineralization of contemporary and/or accumulating younger carbon sources, including Holocene-aged permafrost, thick peat, and lake sediment packages; (2) a progressive decrease in the spatial extent of unmodified Pleistocene-aged yedoma permafrost due to thermokarst and thermo-erosion[56]; or (3) changes in relative contributions from yedoma and non-yedoma thermokarst lakes caused by shifts in emission strengths or lake distributions. Today, the composite age of all thermokarst lakes (3132 ± 731 yr BP, Table 1) is significantly younger than yedoma-type thermokarst lakes alone (7828 ± 3899 yr BP) because 74% of present-day thermokarst lake area is outside the yedoma region, where thermokarst lakes form in comparatively less carbon-rich and/or younger permafrost soils (Table S2). The two forward

modeled atmospheric $\Delta^{14}CH_4$ curves based on each end-member age (Fig. 5) bound a range of possible atmospheric $\Delta^{14}CH_4$ values for comparison to the ice core $\Delta^{14}CH_4$ data.

Thermokarst lakes as a positive feedback to climate warming. While we have tentatively ruled out that lakes were the primary source of abrupt AMC rise, our data do suggest climate-driven lake feedback to warming. Episodes of abrupt warming at 14.7 ka and 11.6 ka (Fig. 3a) triggered ice sheet retreat and permafrost thaw that accelerated both thermokarst and glacial lake formation[23]. Methane release resulting from a rapid expansion in lake area following the Younger Dryas (Fig. 2) likely contributed to a more gradual increase in NH temperature, which followed the initial abrupt rise (11.6 ka, Fig. 3). Radiative forcing of 0.03 W m^{-2} resulting from a 13 Tg CH_4 yr^{-1} increase in thermokarst lake emissions would have warmed the planet by ~0.024 °C over the deglacial period. This constitutes a small positive feedback to warming that likely helped sustain high, early Holocene temperatures during a diminishing phase of solar insolation that began 11 ka[30] (Fig. 3).

Contrary to recent suggestions, our findings provide specific evidence that the emission of methane from permafrost carbon sources functioned as a small positive feedback to deglacial climate warming. Thermokarst lake emission ages represent a mixture of methane derived from substrates of different ages (late Pleistocene, Holocene, contemporary, Fig. 4). Despite uncertainties in carbon-source ages and mixing ratios, net emission ages of thousands of years old (Table 1), and methane sample ages that predominantly exceed lake age (Fig. 6), identify thermokarst lakes as a conduit for release of previously sequestered carbon, and distinguish this source from other components of the contemporary carbon cycle. Regardless of how long this carbon was withheld from contemporary cycling, its reintroduction through climate-driven thermokarst lake formation and subsequent methane production constitutes positive feedback to warming. Furthermore, even if all of the ^{14}C-depleted methane emitted from non-yedoma thermokarst and glacial lakes originated from active layer soil carbon, and not from thawing permafrost soils themselves (false scenario), the release to the atmosphere, especially as methane, still constitutes a permafrost carbon feedback. This is because it represents the mineralization of permafrost region soil organic matter[57] facilitated by the creation of anaerobic environments by permafrost thaw and active layer saturation.

Our bottom-up estimates suggest that thermokarst lakes contributed up to 15 ± 6 Tg CH_4 yr^{-1} to the atmosphere, and constituted a maximum of 9% of the total northern hemisphere source (compared to 17% for all lakes) during the deglacial period. Comparison with ice core data (Fig. 5) shows that at its current analytical precision, $\Delta^{14}C$-CH_4 data from ice cores, unfortunately, cannot provide strong constraints on younger (but still aged relative to contemporaneous $^{14}CO_2$) methane emissions from permafrost systems. We showed that methane emissions from lake sources (Figs. 2, 3) had a delayed response relative to abrupt northern hemisphere warming (as recorded in Greenland ice cores[9]) and peaked at around 11-9 ka. Our bottom-up estimates (Figs. 2, 3) and box modeling results (Fig. 5) provide a target time-period for future ice core measurements (e.g., a more accurate AMC and stable isotopes interpolar gradient that is free from excess CH_4 artifacts from dusty Greenland ice[55]) to test against. Future studies will have greater success disentangling source contributions as these datasets continue to improve.

While our methods aptly constrain both total carbon loss from yedoma permafrost through the formation of new lakes, and the timing of peak methane release, we found that the distribution of
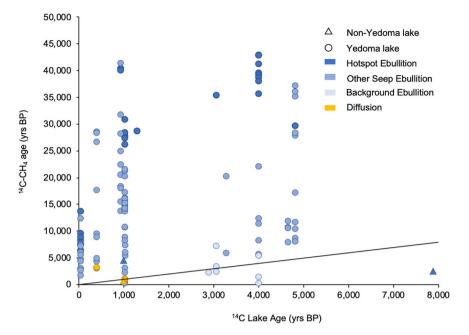
Fig. 6 Ages of thermokarst lake methane samples relative to lake age. The black line depicts a 1:1 relationship between lake age and gas age. Basal lake ages (x-axis) are from Walter ref. [13] and ref. [16]; Lake methane ages (y-axis) are from and ref. [15].

this carbon loss (i.e., relative peak magnitude) during deglaciation was strongly influenced by lake size (Supplementary Information Section 1.2). Changes in thermokarst lake size over time, evidenced by the superposition of smaller lake basins over larger ones throughout the yedoma region[56,58], likely occurred as ice-rich permafrost land surfaces evolved from contiguous uplands favoring lateral expansion, to complex, fragmented networks that provided greater opportunity for lake modification and drainage[33,56]. A better understanding of this phenomenon, and quantification of systematic changes in lake size over time, are necessary to better assess the importance of yedoma thermokarst lake methane emissions during the early deglacial period.

Future permafrost carbon feedback. In light of these new paleoenvironmental records, radiocarbon methane age syntheses, and modeling, we conclude that thermokarst lakes were a positive feedback to climate warming during the last deglaciation, albeit small compared to other new atmospheric methane sources at that time. The last deglaciation provides an imperfect analog for modern warming, however. Today, permafrost is less extensive and permafrost landscapes are geomorphically more mature than at the end of the last glacial period. While some areas are more carbon-rich now compared to the end of the last ice age[37,59] permafrost soils are also, in many places, more protected from warming due to insulation by accumulated peat and vegetation[60]. Still, current rates of anthropogenic warming are two orders of magnitude faster than during the previous glacial-interglacial transition; and 50–140% of the 6 °C global warming that occurred over 8000 years from 18 ka to 10 ka[7,8] is projected to occur in the Arctic in just 80 years under current emissions projections[2]. Hence, models agree that 21st-century warming will likely overwhelm contemporary boundary conditions and result in widespread permafrost loss, leading to the mobilization and decomposition of a large fraction of the permafrost carbon pool[4]. Models of abrupt thaw estimate average 21st-century thermokarst lake emissions of 70 Tg CH_4 yr^{-1} [21], equal to more than four times the maximum emissions from this source during the last deglaciation. Thus, we maintain that thermokarst lakes could again function as conduits for permafrost carbon release that will

create a positive feedback to warming this century. Such feedback is already underway in some locations[13].

Ultimately, much of the 21st-century permafrost carbon feedback will depend on how many new lakes the landscape can support. Models consistently predict an increase in precipitation relative to evapotranspiration in the Arctic, especially in summer[61], suggesting that hydrological conditions will become more favorable for thermokarst-lake formation[33]. However, some regions are experiencing a net lake area loss[62] due to permafrost thaw and the creation of thermo-erosional drainage networks[63–65] or through-going taliks[66]. Since emissions from new thermokarst lake areas are much higher than those from old lakes and drained basis, modeling suggests gross drainage will have to exceed gross lake formation and expansion by a factor of four to seven before the positive permafrost carbon feedback will be reversed[20]. Better predictions of thermokarst lake formation and persistence, and associated methane release, will therefore rely upon enhanced modeling of climate, hydrological and geomorphological interactions under future climate change scenarios.

Future formation of glacial lakes will be constrained to land areas exposed by continued glacier and ice sheet melt. However, increases in methane emissions projected to occur as lake bottom waters warm[67] and ice free-seasons lengthen could be larger for glacial lakes than for thermokarst lakes alone due to their much larger spatial extent.

Conclusion
Here we show that our bottom-up, panarctic lake methane emission estimates are consistent with top-down polar ice core $^{14}CH_4$ constraints, especially when revised lake flux ages based on a new synthesis of radiocarbon data are applied. Lake formation accelerated in response to climate warming, releasing old methane from a mixture of stored (permafrost), and contemporary carbon sources that created a positive climate feedback helping to sustain early Holocene temperature increases. Thermokarst lakes emitted disproportionately more old carbon than glacial lakes. However, new emission estimates from glacial lakes, which dominate the panarctic lake area, were more than double

those from thermokarst lake emissions throughout the majority of the Holocene.

Methods

Lake methane age calculations. To assess the contribution of old carbon to deglacial and Holocene lake emissions, we compiled extensive radiocarbon data[15] associated with various modes of methane emission (diffusive, storage, and ebullition fluxes) for different Arctic lake types and settings (thermokarst lakes formed in Pleistocene-aged yedoma permafrost of North Siberia, Alaska, and Northwest Canada; thermokarst-lakes formed in Holocene-aged permafrost throughout the remainder of the Arctic permafrost region, and panarctic glacial lakes) (Table S1 and Fig. S2). We used these data, along with a previously developed mixing model[6] based on Antarctic ice core Δ^{14}C-CH$_4$ data[6,47] to reevaluate potential methane contributions from old carbon sources associated with permafrost thaw and lake formation during the deglacial period.

Lake basal age extraction. We used a recent compilation of 1207 basal ages and lake origins from past and extant lakes (HiLLBAO), within the domain of glaciation and permafrost extent during the Last Glacial/Permafrost Maximum (https://doi.org/10.1594/PANGAEA.894737)[16] to reconstruct past lake methane emissions. This dataset was gathered primarily from scientific literature descriptions of lake cores, peat cores underlain by lake sediments, and riverbank exposures. Though 95% of records were radiocarbon-dated, robust dates obtained by a variety of methods were accepted. We evaluated the effect of assuming a normal ($1\sigma = 200$ years) or positively skewed (Figs. S4, S5) distribution of dating error for all basal ages included in the dataset on modeled methane emissions (scenarios A and B, respectively, in Figs. 2, 3). We chose this approach to avoid heavy weighting of older radiocarbon dates based on their larger analytical error, and to explore the impact of non-normally distributed dating error on the timing of emission estimates. We acknowledge that basal ages in the dataset could have a bias towards being younger than they really are due to (1) the failure of some coring efforts to penetrate stiff glaciolacustrine sediments overlying true basal sediments; (2) the common interpretation of mineral-organic sediment transitions as indicators of lake formation within the literature; and (3) the inability of a single coring location to account for transgressive lake formation/expansion (i.e., lake formation may have occurred earlier than inundation of the coring site). Applying a positive skew to the distribution of basal age errors allows some assessment of the impact of this possible bias. Other dataset attributes, potential sources of dating error, and spatiotemporal patterns of lake formation are discussed in the original presentation of the dataset[23]. All radiocarbon dates of lake sediments were recalibrated for this study using Calib 7.0[68].

Modeled lake methane emissions presented here are based on distributions of lake basal ages ≤18,000 years old ($n = 1112$ out of the full dataset of 1207 dates). We excluded 95 basal ages for lakes formed earlier than 18,000 years ago and large ice-dammed, proglacial lakes from our database and subsequent lake area and methane emission estimates due to their high spatiotemporal complexity.

Modern lake area extraction. We defined the study domain (Fig. 1) as the panarctic region, including all areas that (1) are affected by permafrost today[69], (2) were affected by permafrost during the Last Permafrost Maximum[26], or (3) were covered by ice sheets during the LGM[70]. This region, falling primarily northward of 35° to 45°, largely overlaps the high latitude region northward of 30° defined in interpolar gradient studies[27,28,54]. Extracted areas of modern lakes present on both formerly glaciated and unglaciated landscapes within our study domain are based on the Global Lakes and Wetland Database (minimum lake size: 0.1 km^2)[71]. We then used the current extent of coastlines and political/geographic or physiographic regions (ESRI Basemap) to separate our study domain into subregions suitable for regional scaling of lake methane emission characteristics (Fig. S3). For each subregion, we determined the areal extents of modern lake distribution based on the Global Lakes and Wetland Database. We used the distributions of different lake types within the dataset[23] to proportionally adjust lake areas by type (Table S2).

Glacial lake methane flux estimates. The majority (88%) of non-thermokarst lakes included in our dataset were formed by a variety of mechanisms directly associated with deglaciation[23]. The remainder (12%) were formed by volcanic, tectonic, carbonate weathering, or other processes. For simplification, we refer to all non-thermokarst lakes as "glacial" lakes in this analysis. To estimate fluxes from these lakes, we adopted a regionalized approach, accounting for strong spatial dynamics in patterns of glacial lake formation related to ice sheet retreat[23]. We used modern lake extents (Table S2) and distributions of glacial lake basal ages[16] to linearly reconstruct glacial lake areas in 100-year timesteps from 18 ka to the present for each subregion of our study domain (Fig. S3). This approach assumes the establishment of differently sized lakes with a consistent mean size (i.e., no systematic variation) over time (Supplementary Information Section 1.2). To partially account for glacial lake area loss caused by climate drying and isostatic rebound since deglaciation, we modified rates of glacial lake formation using a lake drainage function. We derived this function from glacial lake termination ages within our dataset obtained from dated transitions in peat core or sediment exposure stratigraphy ($n = 40$). This allowed reconstructed glacial lake areas used

for scaling methane emissions to exceed modern lake extents during the early Holocene.

Following approaches previously adopted for Holocene peatland emissions[29], we applied a temperature correction to measured, present-day annual methane fluxes (sum of measured annual diffusion, storage, and ebullition fluxes) from glacial lakes (10.1 ± 4.8 g CH$_4$ m^{-2} yr^{-1}, Table S1) in 100-year timesteps to reflect the ecosystem-level influence of reconstructed changes in temperature[72,73] on methane production using the relationship derived by ref. [36]. We assumed these temperature-corrected areal flux rates were representative across the domain, and multiplied the areal flux rate by the reconstructed lake areas in 100-year timesteps to estimate methane emissions from panarctic glacial lakes through time.

Thermokarst lake methane flux estimates. Thermokarst lakes form when ice-rich permafrost thaws, causing ground subsidence and the creation of a water-impounding depression. We used an existing mass balance-constrained approach[37] as the basis for estimating methane emissions from thermokarst lakes in the yedoma region; however, we updated the model to reflect the temporal distribution of 60% more thermokarst lake formation dates available through the High-Latitude Lake Basal Ages and Origins (HiLLBAO) database[16]. Briefly, we used a mass-balance derived estimate of 95 ± 34 Pg C[35] to constrain cumulative Pleistocene-aged methane produced in thermokarst lakes from 18 ka to the present. Following long-term laboratory incubation observations and earlier modeling[37,74], we assumed a 1:1 stoichiometric relationship between carbon dioxide and methane produced from the labile fraction of thawed yedoma. This ratio is also consistent with the theoretical chemistry of steady-state methanogenesis with cellulose as the primary substrate[75]. We then distributed the pool of yedoma permafrost carbon lost as methane in 100-year timesteps to capture end-member scenarios of carbon release trajectories: (1) solely based on rates of new thermokarst lake formation in each timestep following observations that the majority of yedoma-carbon derived carbon is emitted within a century of thermokarst-induced inundation along shorelines[13] (scenario B in Figs. 2, 3) or (2) in combination with a numerically simulated flux trajectory that extends methane produced from thawed yedoma deposits in thermokarst lakes for the first 1200 years after lake initiation following ref. [18] (Fig. S6, scenario A in Figs. 2, 3). Though we identified changes in yedoma thermokarst lake size as an important source of potential uncertainty in the timing and magnitude of modeled deglacial lake emissions (Supplementary Information Section 1.2), we could not reliably estimate its impact on our modeling results due to a paucity of data.

We estimated Holocene-aged methane emissions that dominate in late-stage yedoma lakes and non-yedoma thermokarst lakes in 100-year timesteps using modern annual fluxes observed in these environments (6.8 ± 4.4 g CH$_4$ m^{-2} yr^{-1}, Table S1) in the yedoma region[38,44,45]. This value was modified in 100-year timesteps to account for changes in temperature as in methods section 1.4. After 3570 ± 1160 years, lakes were assumed to drain. The 3600-year average "lifespan" of thermokarst lakes was determined by stratigraphic analyses of multiple lake initiation and drainage sequences in yedoma exposures ($n = 6$ date pairs; data from ref. [37], ref. [76] and Walter Anthony, unpublished data). Post-drainage emissions from alases (drained lake basins), often fall under a wetland classification. To avoid double counting with peatland methane inventories, we excluded post-lake drainage emissions and emissions from vegetated lake margins from our analysis. Our analysis applies only to open-water lake areas.

We used a similar method to calculate emissions from thermokarst lakes that formed on various other permafrost substrates outside of the yedoma region (e.g., in non-glaciated areas of western Siberia, central Asia, northern Alaska, and Europe situated within the last permafrost maximum extent, here termed "non-yedoma" thermokarst lakes, with a modern area of 126,685 km^2 (Table S2). We linearly reconstructed non-yedoma lake area in 100-year timesteps using the distribution of thermokarst lake initiation ages. We also assumed that the average age of existing thermokarst lakes in the dataset represents the typical "lifespan" of these lakes (8700 ± 5200 years). We applied an annual flux rate of 6.8 ± 4.4 g CH$_4$ m^{-2} yr^{-1} (Table S1) mineralized from predominantly younger permafrost and contemporary carbon substrates fueling methane production in non-yedoma environments (Fig. 6). This flux rate was temperature-adjusted and multiplied by reconstructed lake areas in each 100-year timestep to estimate non-yedoma thermokarst lake emissions over time.

Forward atmospheric Δ^{14}CH$_4$ box model. A detailed description of the box model is given in the Supplementary Material of ref. [6]. In brief, atmospheric CH$_4$ burden is reconstructed from CH$_4$ mole fraction data in ice cores. The lifetime of atmospheric CH$_4$ is assumed to be 10.05 years. From 18 to 7.7 ka, CH$_4$ mole fractions from NEEM and WAIS ice cores[77] are used to calculate the global CH$_4$ source strength (Q_{tot}). From 7.7 ka onwards, we used CH$_4$ mole fraction compilation from Beck et al.[78] The isotope mass balance of ^{14}C-CH$_4$ in the atmosphere is given by

$$^{14}C_{atm}Q_{tot} = {}^{14}C_{TKL}Q_{TKL} + {}^{14}C_{intcal}Q_{mod} \qquad (1)$$

$$Q_{tot} = Q_{tot} + Q_{tot} \qquad (2)$$

where $^{14}C_{atm}$ is the atmospheric Δ^{14}CH$_4$, Q_{tot} is the global CH$_4$ emissions, $^{14}C_{TKL}$ is the ^{14}C activity of CH$_4$ emissions from thermokarst lakes (Q_{TKL}, which is

estimated in this study), and $^{14}C_{intcal}$ is the ^{14}C activity of contemporaneous/modern CH_4 emissions (Q_{mod}). All ^{14}C terms in Eq. 1 are in pMC (percent modern carbon) unit while the flux terms (Q) are in Tg CH_4 yr^{-1}. We assumed that at the time of emission, $^{14}C_{mod}$ is equal to ^{14}C activity of $^{14}CO_2$ derived from IntCal20[79]. As discussed above, we ran two scenarios for $^{14}C_{TKL}$, one assuming $^{14}CH_4$ activity of 3132 years and 7828 years old relative to contemporaneous emissions. This assumption is implemented using Eq. 3.

$$^{14}C_{TKL}(t) = {}^{14}C_{intcal}(t + t_{TKL}) \cdot e^{-\lambda t_{TKL}} \qquad (3)$$

where t_{TKL} is either 3132 yr or 7828 yr and λ is the ^{14}C decay constant in yr^{-1}.

Climate forcing. We used equations published in the 2013 IPCC report[80] to calculate the radiative forcing and global temperature increase resulting from lake methane emissions estimated in this study. We assumed a global mean equilibrium temperature change following a doubling of atmospheric CO_2 of 3 °C.

Data availability
The High-Latitude Lake Basal Ages and Origins (HiLLBAO) dataset utilized in this study is available in the PANGAEA repository (https://doi.org/10.1594/PANGAEA.894737)[16]. The compilation of lake methane radiocarbon ages (https://doi.org/10.18739/A25717Q0T)[15] and estimates of panarctic lake methane emissions (https://doi.org/10.18739/A2TX3577N)[81] are also publicly available. All other data supporting the findings of this study are available within the paper and its Supplementary Information.

Code availability
Algorithms used to produce the results of this study are available from the corresponding author upon request.

References
1. Rantanen, M. et al. The Arctic has warmed nearly four times faster than the globe since 1979. *Commun. Earth Environ.* **3**, 168 (2022).
2. Cai, Z. et al. Arctic warming revealed by multiple CMIP6 models: evaluation of historical simulations and quantification of future projection uncertainties. *J. Clim.* **34**, 4871–4892 (2021).
3. Hugelius, G. et al. Estimated stocks of circumpolar permafrost carbon with quantified uncertainty ranges and identified data gaps. *Biogeosciences* **11**, 6573–6593 (2014).
4. Schuur, E. A. et al. Climate change and the permafrost carbon feedback. *Nature* **52**, 171–179 (2015).
5. Rogelj, J. et al. Energy system transformations for limiting end-of-century warming to below 1.5°C. *Nat. Clim. Chang.* **5**, 519–527 (2015).
6. Dyonisius, M. N. et al. Old carbon reservoirs were not important in the deglacial methane budget. *Science* **367**, 907–910 (2020).
7. Tierney, J. E. et al. Glacial cooling and climate sensitivity revisited. *Nature* **584**, 569–573 (2020).
8. Osman, M. B. et al. Globally resolved surface temperatures since the Last Glacial Maximum. *Nature* **599**, 239–244 (2021).
9. Brook, E. J., Harder, S., Severinghaus, J., Steig, E. J. & Sucher, C. M. On the origin and timing of rapid changes in atmospheric methane during the last glacial period. *Glob. Biogeochem. Cycles* **14**, 559–572 (2000).
10. Rhodes, R. H. et al. Enhanced tropical methane production in response to iceberg discharge in the North Atlantic. *Science* **348**, 1016–1019 (2015).
11. Elder, C. D. et al. Greenhouse gas emissions from diverse Arctic Alaskan lakes are dominated by young carbon. *Nat. Clim. Chang.* **8**, 166–171 (2018).
12. Dean, J. F. et al. East Siberian Arctic inland waters emit mostly contemporary carbon. *Nat. Comm.* **11**, 1–10 (2020).
13. Walter Anthony, K. M. et al. Decadal-scale hotspot methane ebullition within lakes following abrupt permafrost thaw. *Environ. Res. Lett.* **16**, 035010 (2021).
14. Strauss, Jr, Y. et al. Circum-Arctic Map of the Yedoma Permafrost Domain. *Cryospheric Sci.* https://doi.org/10.3389/feart.2021.758360 (2022)
15. Walter Anthony, K. Radiocarbon ages of methane in arctic and boreal lakes (2003-2017). Arctic Data Center https://doi.org/10.18739/A25717Q0T (2023).
16. Brosius, L. S. et al. High-latitude Lake Basal ages and origins *PANGAEA* https://doi.org/10.1594/PANGAEA.894737 (2018).
17. Olefeldt, D. et al. Circumpolar distribution and carbon storage of thermokarst landscapes. *Nat. Commun.* **7**, 13043 (2016).
18. Kessler, M. A., Plug, L. J. & Walter Anthony, K. M. Simulating the decadal-to millennial-scale dynamics of morphology and sequestered carbon
19. Walter Anthony, K. M. et al. Methane emissions proportional to permafrost carbon thawed in Arctic lakes since the 1950s. *Nat. Geosci.* **9**, 679–682 (2016).
20. Walter Anthony, K. M. et al. 21st-century modeled permafrost carbon emissions accelerated by abrupt thaw beneath lakes. *Nat. Commun.* **9**, 3262 (2018).
21. Turetsky, M. R. et al. Carbon release through abrupt permafrost thaw. *Nat. Geosci.* **13**, 138–143 (2020).
22. Smith, L. C., Sheng, Y. & MacDonald, G. M. A first panarctic assessment of the influence of glaciation, permafrost, topography and peatlands on northern hemisphere lake distribution. *Permafrost Periglac. Process.* **18**, 201–208 (2007).
23. Brosius, L. B. et al. Spatiotemporal patterns of northern lake formation since the Last Glacial Maximum. *Quat. Sci. Rev.* **253**, 106773 (2021).
24. Walter, K. M., Edwards, M. E., Grosse, G., Zimov, S. A. & Chapin, F. S. Thermokarst lakes as a source of atmospheric CH_4 during the last deglaciation. *Science* **318**, 633–636 (2007).
25. Brosius, L. S. et al. Using the deuterium isotope composition of permafrost meltwater to constrain thermokarst lake contributions to atmospheric CH_4 during the last deglaciation. *J. Geophys. Res.* **117**, G01022 (2012).
26. Lindgren, A., Hugelius, G., Kuhry, P., Christensen, T. R. & Vandenberghe, J. GIS-based maps and area estimates of northern hemisphere Permafrost extent during the Last Glacial Maximum. *Permafrost Periglac. Process.* **27**, 6–16 (2016).
27. Baumgartner, M. et al. High-resolution interpolar difference of atmospheric methane around the Last Glacial Maximum. *Biogeosciences* **9**, 3961–3977 (2012).
28. Yang, J., Ahn, J., Brook, E. J. & Ryu, Y. Atmospheric methane control mechanisms during the early Holocene. *Clim. Past* **13**, 1227–1242 (2017).
29. Treat, C. C. et al. The role of wetland expansion and successional processes in methane emissions from high-latitude wetlands during the Holocene. *Quat. Sci. Rev.* **257**, 106864 (2021).
30. Berger, A. & Loutre, M. F. Insolation values for the climate of the last 10 million years. *Quat. Sci. Rev.* **10**, 297–317 (1991).
31. North Greenland Ice Core Project members. High-resolution record of Northern Hemisphere climate extending into the last interglacial period. *Nature* **431**, 147–151 (2004).
32. Grosse, G., Jones, B., Arp, C. Thermokarst lakes, drainage, and drained basins. In *Treatise on Geomorphology* (eds Shroder, J., Giardino, R. & Harbor, J.) vol. 8, 325–353 (Academic Press, San Diego, CA, 2013).
33. van Huissteden, J. et al. Methane emissions from permafrost thaw lakes limited by lake drainage. *Nat. Clim. Change* **1**, 119–123 (2011).
34. Dyke, A. S. An outline of North American deglaciation with emphasis on central and northern Canada. *Dev. Quat. Sci.* **2**, 371–405 (2004)
35. Hughes, A. L. C., Gyllencreutz, R., Lohne, S., Mangerud, J. & Svendsen, J. I. The last Eurasian ice sheets—a chronological database and time-slice reconstruction, DATED-1. *Boreas* **45**, 1–45 (2016).
36. Yvon-Durocher, G. et al. Methane fluxes show consistent temperature dependence across microbial to ecosystem scales. *Nature* **507**, 488–491 (2014).
37. Walter Anthony, K. M. et al. A shift of thermokarst lakes from carbon sources to sinks during the Holocene epoch. *Nature* **511**, 452–456 (2014).
38. Wik, M., Varner, R. K., Anthony, K. W., MacIntyre, S. & Bastviken, D. Climate-sensitive northern lakes and ponds are critical components of methane release. *Nat. Geosci.* **9**, 99–105 (2016).
39. Matthews, E. et al. Methane emission from high latitude lakes: methane-centric lake classification and satellite-driven annual cycle of emissions. *Sci. Rep.* **10**, 12465 (2020).
40. Walter, K. M., Chanton, J. P., Chapin, F. S. III, Schuur, E. A. G. & Zimov, S. A. Methane production and bubble emissions from arctic lakes: Isotopic implications for source pathways and ages. *J. Geophys. Res.* **113**, G00A08 (2008).
41. Walter, K. M., Zimov, S. A., Chanton, J. P., Verbyla, D. & Chapin, F. S. Methane bubbling from Siberian thaw lakes as a positive feedback to climate warming. *Nature* **443**, 71–75 (2006).
42. Heslop, J. K. et al. A synthesis of methane dynamics in thermokarst lake environments. *Earth Sci. Rev.* **210**, 103365 (2020).
43. Greene, S., Walter Anthony, K. M., Archer, D., Sepulveda-Jauregui, A. & Martinez-Cruz, K. Modeling the impediment of methane ebullition bubbles by seasonal lake ice. *Biogeoscience* **11**, 6791–6811 (2014).
44. Townsend-Small, A., Åkerström, F., Arp, C. D. & Hinkel, K. M. Spatial and temporal variation in methane concentrations, fluxes, and sources in lakes in Arctic Alaska. *J. Geophys. Res. Biogeosci.* **122**, 2966–2981 (2017).
45. Sepulveda-Jauregui, A., Walter Anthony, K. M., Martinez-Cruz, K., Greene, S. & Thalasso, F. Methane and carbon dioxide emissions from 40 lakes along a north–south latitudinal transect in Alaska. *Biogeosciences* **12**, 3197–3223 (2015).
46. Elder, C. D. et al. Seasonal sources of whole-lake CH_4 and CO_2 emissions from Interior Alaskan thermokarst lakes. *J. Geophys. Res. Biogeosci.* **124**, 1209–1229 (2019).
47. Petrenko, V. V. et al. Minimal geological methane emissions during the Younger Dryas-Preboreal abrupt warming event. *Nature* **548**, 443–446 (2017).

48. Möller, L. et al. Independent variations of CH₄ emissions and isotopic composition over the past 160,000 years. *Nat. Geosci.* **6**, 885–890 (2013).

49. Bock, M. et al. Glacial/interglacial wetland, biomass burning, and geologic methane emissions constrained by dual stable isotopic CH₄ ice core records. *Proc. Natl Acad. Sci. USA* **114**, E5778–E5786 (2017).

50. Winterfeld, M. et al. Deglacial mobilization of pre-aged terrestrial carbon from degrading permafrost. *Nat. Commun.* **9**, 3666 (2018).

51. Walter Anthony, K. M., Anthony, P., Grosse, G. & Chanton, J. Geologic methane seeps along boundaries of Arctic permafrost thaw and melting glaciers. *Nat. Geosci.* **5**, 419–426 (2012).

52. Chuvilin, E. et al. A gas-emission crater in the Erkuta River Valley, Yamal Peninsula: characteristics and potential formation model. *Geosciences* **10**, 170 (2020).

53. Carrivick, J. L. & Tweed, F. S. Proglacial lakes: character, behaviour and geological importance. *Quat. Sci. Rev.* **78**, 34–52 (2013).

54. Chappellaz, J. et al. Changes in the atmospheric CH₄ gradient between Greenland and Antarctica during the Holocene. *J. Geophys. Res.* **102**, 15987–15997 (1997).

55. Lee, J. E. et al. Excess methane in Greenland ice cores associated with high dust concentrations. *Geochim. Cosmochim. Acta* **270**, 409–430 (2020).

56. Morgenstern, A., Grosse, G., Günther, F., Fedorova, I. & Schirrmeister, L. Spatial analyses of thermokarst lakes and basins in Yedoma landscapes of the Lena Delta. *Cryosphere* **5**, 849–867 (2011).

57. Koven, C. D. et al. A simplified, data-constrained approach to estimate the permafrost carbon–climate feedback. *Phil. Trans. R. Soc. A.* **373**, 20140423 (2015).

58. Jones, M. C., Grosse, G., Jones, B. M. & Walter Anthony, K. M. Peat accumulation in drained thermokarst lake basins in continuous, ice-rich permafrost, northern Seward Peninsula, Alaska. *J. Geophys. Res. Biogeosci.* **117**, G2 (2012).

59. Lindgren, A., Hugelius, G. & Kuhry, P. Extensive loss of past permafrost carbon but a net accumulation into present-day soils. *Nature* **560**, 219–222 (2018).

60. Mann, D. H., Groves, P., Reanier, R. E. & Kunz, M. L. Floodplains, permafrost, cottonwood trees, and peat: What happened the last time climate warmed suddenly in arctic Alaska? *Quat. Sci. Rev.* **29**, 3812–3830 (2010).

61. Lique, C., Holland, M. M., Dibike, Y. B., Lawrence, D. M. & Screen, J. A. Modeling the Arctic freshwater system and its integration in the global system: lessons learned and future challenges. *J. Geophys. Res. Biogeosci.* https://doi.org/10.1002/2015JG003120 (2016).

62. Webb, E. E. et al. Permafrost thaw drives surface water decline across lake-rich regions of the Arctic. *Nat. Clim. Chang.* **12**, 841–846 (2022).

63. Liljedahl, A. et al. Panarctic ice-wedge degradation in warming permafrost and its influence on tundra hydrology. *Nat. Geosci.* **14**, 312–318 (2016).

64. Jones, B. M. et al. Lake and drained lake basin systems in lowland permafrost regions. *Nat. Rev.* **3**, 85–95 (2022).

65. Arp, C. D., Jones, B. M., Liljedahl, A. K., Hinkel, K. M. & Welker, J. A. Depth, ice thickness, and ice-out timing cause divergent hydrologic responses among Arctic lakes. *Water Resour. Res.* **51**, 9379–9401 (2015).

66. Yoshikawa, K. & Hinzman, L. Shrinking thermokarst ponds and groundwater dynamics in discontinuous permafrost near Council, Alaska. *Permafrost Periglac. Process.* **14**, 151–160 (2003).

67. Jansen, J. et al. Global increase in methane production under future warming of lake bottom waters. *Glob. Change Biol.* **28**, 5427–5440 (2022).

68. Stuiver, M. & Reimer, P. J. Extended ¹⁴C data base and revised CALIB 3.0 ¹⁴C age calibration program. *Radiocarbon* **35**, 215–230 (1993).

69. Brown, J., Ferrians Jr, O. J., Heginbottom, J. A. & Melnikov, E. S. Circum-Arctic map of permafrost and ground-ice conditions. National Snow and Ice Data Center/World Data Center for Glaciology. Digital media (1998).

70. Ehlers, J. & Gibbard, P. L. Extent and chronology of glaciations. *Quat. Sci. Rev.* **22**, 1561–1568 (2003).

71. Lehner, B. & Döll, P. Development and validation of a global database of lakes, reservoirs and wetlands. *J. Hydrol.* **296**, 1–22 (2004).

72. Shakun, J. D. et al. Global warming preceded by increasing carbon dioxide concentrations during the last deglaciation. *Nature* **484**, 49–54 (2012).

73. Marcott, S. A., Shakun, J. D., Clark, P. U. & Mix, A. C. A reconstruction of regional and global temperature for the past 11,300 years. *Science* **339**, 1198–1201 (2013).

74. Knoblauch, C., Beer, C., Sosnin, A., Wagner, D. & Pfeiffer, E. M. Predicting long-term carbon mineralization and trace gas production from thawing permafrost of Northeast Siberia. *Glob. Change Biol.* **19**, 1160–1172 (2013).

75. Conrad, R., Klose, M. & Claus, P. Pathway of CH₄ formation in anoxic rice field soil and rice roots determined by 13C-stable isotope fractionation. *Chemosphere* **47**, 797–806 (2002).

76. Farquharson, L. et al. Facies analysis of Yedoma thermokarst lakes on the northern Seward Peninsula, Alaska. *Sed. Geol.* **340**, 25–37 (2016).

77. Rosen J. L. *Augmenting and Interpreting Ice Core Greenhouse Gas Records*. PhD thesis, Oregon State Univ. (2014).

78. Beck, J. et al. Bipolar carbon and hydrogen isotope constraints on the Holocene methane budget. *Biogeosciences* **15**, 7155–7175 (2018).

79. Reimer, P. J. et al. The IntCal20 northern hemisphere radiocarbon age calibration curve (0–55 cal kBP). *Radiocarbon* **62**, 725–757 (2020).

80. Myhre, G. et al. in *Climate Change 2013: The Physical Science Basis. Contribution of Working Group I to the Fifth Assessment Report of the Intergovernmental Panel on Climate Change* (eds Stocker, T. F. et al.) Ch. 8 (Cambridge Univ. Press, 2014).

81. Brosius, L. et al. Estimates of panarctic lake methane emissions from 18ka to present. Arctic Data Center https://doi.org/10.18739/A2TX3577N (2023)

82. Amante, C. & Eakins, B. W. ETOPO1 1 arc-minute global relief model: procedures, data sources and analysis. US Department of Commerce, National Oceanic and Atmospheric Administration, National Environmental Satellite, Data, and Information Service, National Geophysical Data Center, Marine Geology and Geophysics Division (2009).

83. Blunier, T., Chappellaz, J. A., Schwander, J., Stauffer, B. & Raynaud, D. Variations in atmospheric methane concentration during the Holocene epoch. *Nature* **374**, 46–49 (1995).

84. Chappellaz, J. et al. High-resolution glacial and deglacial record of atmospheric methane by continuous-flow and laser spectrometer analysis along the NEEM ice core. *Clim. Past* **9**, 2579–2593 (2013).

85. Rhodes, R. H. et al. Continuous methane measurements from a late Holocene Greenland Core: Atmospheric and in-situ signals. *Earth Planet. Sci. Lett.* **368**, 9–19 (2015).

Acknowledgements

Author contributions

L.S.B. and K.M.W.A. had primary responsibility for design, analysis, and writing; C.C.T., K.M.W.A., and G.G. contributed to the datasets. C.C.T., G.G., and M.C.J. assisted with methods and analysis. M.D. conducted ¹⁴CH₄ forward modeling. All authors contributed to the interpretation and writing.

Competing interests

The authors declare no competing interests.

Additional information

Supplementary information The online version contains supplementary material available at https://doi.org/10.1038/s43247-023-00930-2.

Correspondence and requests for materials should be addressed to L. S. Brosius.

Peer review information *Communications Earth & Environment* thanks the other, anonymous, reviewer(s) for their contribution to the peer review of this work. Primary Handling Editor: Aliénor Lavergne.

Reprints and permission information is available at http://www.nature.com/reprints

Publisher's note Springer Nature remains neutral with regard to jurisdictional claims in published maps and institutional affiliations.